The General Isothermal Oxidation Behavior of Cu-8Cr-4Nb

L.U.J.T. Ogbuji
QSS, Inc., NASA Glenn Research Center, Cleveland OH 44135

Abstract
Oxidation kinetics of Cu-8Cr-4Nb was investigated by TGA exposures between 500 and 900°C (at 25-50°C intervals) and the oxide scale morphologies examined by microscopy and micro-analysis. Because Cu-8Cr-4Nb is comprised of fine Cr_2Nb precipitates in a Cu matrix, the results were interpreted by comparison with the behavior of copper (OFHC) and "NARloy-Z" (a rival candidate material for thrust cell liner applications in advanced rocket engines) under the same conditions. While NARloy-Z and Cu exhibited identical oxidation behavior, Cu-8Cr-4Nb differed markedly in several respects: below ~700°C its oxidation rates were significantly lower than those of Cu; At higher temperatures its oxidation rates fell into two categories: an initial rate exceeding that of Cu, and a terminal rate comparable to that of Cu. Differences in oxide morphologies paralleled the kinetic differences at higher temperature: While NARloy-Z and Cu produced a uniform oxide scale of Cu_2O inner layer and CuO outer layer, the inner (Cu_2O) layer on Cu-8Cr-4Nb was stratified, with a highly porous/spongy inner stratum (responsible for the fast initial kinetics) and a dense/blocky outer stratum (corresponding to the slow terminal kinetics). Single and spinel oxides of Nb and Cr were found at the interface between the oxide scale and Cu-8Cr-4Nb substrate and it appears that these oxides were responsible for its suppressed oxidation rates at the intermediate temperatures. No difference was found between Cu-8Cr-4Nb oxidation in air and in oxygen at 1.0 atm.

Introduction

The combustion chambers in hypersonic engines are subject to severe mechanical and thermal loads and must be lined with materials of high thermal conductivity and excellent high-temperature mechanical properties. Copper alloys are best suited to that application, and the main combustion chamber of the space shuttle is lined with a Cu-Ag-Zr alloy designated "NARloy-Z", a solution-strengthened alloy with 3 wt. % Ag and 0.5 wt % Zr in Cu. For future reusable launch vehicles a leading candidate for thrust-cell liner is a Cu-8Cr-4Nb alloy designated "GRCop-84" (for NASA Glenn Research Center, where it was developed in conjunction with neighboring Case Western Reserve University). This alloy is a fine dispersion of 14 vol. % Cr_2Nb in Cu, and is characterized by markedly improved mechanical properties without significant reduction of thermal conductivity [1].

Oxidation is always an issue in engine applications, and especially so in these alloys. The Cu matrix of Cu-8Cr-4Nb has poor oxidation resistance, while the chromium content is

both inadequate for Cr_2O_3 protection. Copper and its alloys are known to undergo an oxidation-related damage known as 'blanching', in which cycles of oxidation-reduction produce localized ratcheting degradation resulting in hot spots, pores, and cracks. Rocket engines and combustors lined with Cu alloys and fuelled with H_2-O_2 mixtures present near-ideal conditions for blanching occurrence. While blanching requires a localized fluctuation of thermodynamic conditions [2], its inception lies in oxidation; hence it is important to understand the oxidation behavior of Cu-8Cr-4Nb and related materials.

Copper is of great importance in various industries, and its oxidation behavior has been the subject of many studies. A review by Ronnquist and Fischmeister [3], categorized the wide spectrum of oxidation behavior exhibited by Cu under various conditions. Park and Natesan [4] mapped out Cu oxidation kinetics in three temperature regimes, concluding that surface transport was dominant at low temperatures (below ~500°C), grain boundary diffusion at intermediate temperatures, and bulk diffusion above ~700°C. Whereas it used to be merely assumed, largely from consideration of activation energies, that diffusion of copper ions to the oxide surface was rate determining [3,4], more direct evidence for that mechanism is now available from observed effects of externally applied electric charges on scale growth kinetics [5,6]. The Cu-Cr-Nb composition field is less well understood.

Chiang and co-workers have evaluated the oxidation resistance of Cu-Nb and Cu-Cr coatings proposed for rocket engine applications [7-9]. Using minicomposites made by co-deposition of the elemental constituents from vapor phase or by sputtering, they found that: (1) Cu-Nb formed a non-protective duplex scale, with the thickening of CuO/Cu_2O at the surface controlled by outward diffusion of Cu, while inward diffusion of oxygen controlled the growth of a poorly consolidated subscale comprised of niobium oxides (Nb_2O_5 and $CuNb_2O_6$); (2) in Cu-Cr a Cr content of 15 - 30 vol % was necessary to assure formation of a continuous and protective Cr_2O_3 top scale.

In a study of Cu-8Cr-4Nb oxidation in air from 482 to 816 °C, Chiang and Grimmett found two regimes of different activation energies. Parabolic rate constants for oxidation of Cu-8Cr-4Nb were found to be slower than those for Cu between 482 °C and 816 °C,

the rate constants ($k_{p,,}$ in gm^2/cm^4h) differing by two orders of magnitude at ~650 °C; however, the oxidation rates of the two materials converged at the high and low ends of that temperature interval [10]. That is an interesting result because the oxidation behavior of other Cr_2Nb-containing alloys [11] and of Cu-Cr and Cu-Nb [7-9] give no indication that the Cr_2Nb precipitates in Cu-8Cr-4Nb might confer any oxidative advantage. In any case, even the complete oxidation of the 8 at% Cr in this alloy would be insufficient to provide complete Cr_2O_3 coverage. Yet the results of Chiang and Grimmett indicate that something else is going on besides oxidation of the Cu matrix. Hence, the reason for the oxidative superiority of Cu-8Cr-4Nb remains unclear; and the aim of this paper is to examine its oxidation behavior vis-à-vis that of NARloy-Z and, especially, pure Cu.

Procedure

The materials examined in this study were: Cu-8Cr-4Nb bars containing a slight excess of Cr (with a Cr/Nb atomic ratio of 2.05 to prevent hydride formation by ensuring all Nb is tied up as Cr_2Nb), NARloy-Z bars, and Cu bars obtained as commercial OFHC-Cu. Test specimens were cut into disks 20 mm in diameter and 1.0 mm thick, with a 3mm hole near the rim for hanging, and polished to 800-grit final smoothness. Oxidation was performed in a thermogravimetric analyzer (TGA), the coupons hanging from a sapphire wire inside the 25mm-diameter inner quartz tube of the TGA. The oxidant was purified and dried oxygen (and in some cases air) at 1.0 atm. flowing at 100 cm^3/minute.

Oxidation temperatures were 50°C apart from 500 to 650°C and above 850°C, but the intervals were narrowed to 25°C for Cu-8Cr-4Nb in the temperature regimes (700-850°C) where the kinetics were found to be most sensitive to temperature. Weight changes were acquired continuously by a Cahn 1000 electrobalance with a 100μg sensitivity. Each test lasted 50 H, a much longer duration than the expected service lifetimes of rocket liners. The long duration was chosen in an effort to grow oxide scales that could be handled and studied; trials for shorter times (0.5, 1.0, 2.0, 5.0, 10, and 20 H) yielded oxides that flaked off and curled up upon removal of the sample. Cohesion of the oxide scale improved with longer oxidation duration.

Oxidized samples were sectioned and examined by standard metallographic techniques, including XRD, SEM and EDS. Rigorous analyses of the TGA data for significant changes in parabolic oxidation rate constant, k_p, were performed by Real World Quality Systems of Rocky River, Ohio.

Results and Discussion

Oxidation Kinetics

Copper is an important reference material in this study, and accurate reproduction of literature results for its oxidation will lend fidelity to comparisons made in this paper. Fig. 1 is an Arrhenius plot of data obtained for Cu oxidation kinetics in oxygen. Two regimes are evident: one at high temperatures with an activation energy of 150 kJ/mol (1.55 eV), and another at lower temperatures with an activation energy of ~85 kJ/mol (0.88 eV). This is in very good agreement with the results of Park and Natesan [4], who reported activation energies of 1.79 eV and 0.87 eV, respectively, for the two regimes. (They also found an activation energy of 2.32 eV for a third regime, below 450°C, which was not explored in this study.) The oxidation behavior of NARloy-Z was just as simple. Fig. 2 is a parabolic plot of the data for oxidation of NARloy-Z and Cu in O_2 at 600 and 800°C. It is typical of the results obtained for these two materials at low and high temperatures, respectively. The two curves are coincident at the lower temperature and also almost identical at the higher temperature. Clearly, there is little difference in the oxidation kinetics of NARloy-Z and Cu. In contrast, Cu-8Cr-4Nb oxidation exhibited much complexity.

Specific weight gain is plotted in Fig. 3 as a function of the square root of exposure time for Cu-8Cr-4Nb oxidation at three representative temperatures. (The classification of temperature regimes in this paper is in conformity with terminology in the literature: i.e. paralleling – but not necessarily coincident with – the regimes for Cu [3,4].) At the low temperatures (exemplified by 550°C in Fig. 3) the kinetics were found to be parabolic, while at higher temperatures they may be called "quasi-parabolic", with the following meaning: At intermediate temperatures (700°C) the kinetics oscillated about a mean slope in a manner that is consistent with occasional oxide spallation during its growth; at high

temperature (850°C), in addition to the indication of dynamic spallation, the plots were best fitted as two separate kinetic regimes indicated by the superposed dotted lines. That the slopes of lines **I** and **II** are significantly different will be taken up below. Note, also, that while oscillation of the plots suggests some spallation during oxidation, the effect is not large enough to obscure the gross trends of weight gain. For instance, the plots do not flatten out to become sub-parabolic [12] or dip into the terminal weight-loss behavior commonly observed when oxide growth is diminished by concomitant oxide loss through significant spallation [13] or recession [14,15]. Therefore, for the purpose of discussing kinetics, Cu-8Cr-4Nb oxidation may be said to obey parabolic behavior, and Arrhenius plots may be used to analyze the kinetics.

Fig. 4 shows that the oxidation behavior of Cu-8Cr-4Nb was substantially the same in air and O_2. Ignoring for now the splitting of O_2 oxidation data into two branches at higher temperatures (top left), the significance of which will be discussed later, the results in O_2 (diamonds) are practically coincident with those obtained in air (circles). Hence, allusions in this paper to Cu-8Cr-4Nb oxidation behavior in oxygen should be understood to apply to air also. Besides bifurcation, the O_2 data in Fig. 4 exhibit substantial scatter. Still, as explained earlier, the overall trends are clear enough for meaningful determination of k_p values. With these qualifications in mind, the oxidation behavior of Cu-8Cr-4Nb will now be compared with that of Cu and NARloy-Z.

A comparison is shown in Fig. 5, in which the Cu-8Cr-4Nb data for each temperature have been simplified by averaging. The point of interest in this figure is that, while the oxidation rates (k_p values) for NARloy-Z and Cu are coincident at all temperatures, those of Cu-8Cr-4Nb are slower at intermediate temperatures (500~650°C) by an order of magnitude; above ~700°C oxidation kinetics of all three materials converge. This agrees with the observation of Chiang and Grimmett [10]. In Fig. 6 the data for Cu-8Cr-4Nb oxidation are shown in full, revealing the complexity of its behavior. Below ~700°C, as noted, its parabolic rate constants are up to ten times lower than those for Cu. The slope shown for Cu-8Cr-4Nb in this figure (calculated by regression with $R^2 = 0.968$) indicates an activation energy of ~98 kJ/mol, which is close to the 85 kJ/mol for Cu in this regime.

The behavior of Cu-8Cr-4Nb at high temperatures is characterized by the appearance of two kinetic branches. The lower branch represents oxidation rates similar to those of Cu, while the upper branch represents rates 4-5 times faster than for Cu. The two branches correspond to fast initial kinetics and slow terminal kinetics in Cu-8Cr-4Nb oxidation, as illustrated in Fig. 7 and Table 1 for 800°C. The oxide microstructures in Fig. 7 correlate with the different kinetic zones, as indicated: Image I is from the oxide region nearest to the substrate and represents early growth, its spongy morphology being evident in the higher-magnification image below; Image II is from the outermost region of the scale and represents the dense, final-stage oxide. Clearly, the initial stage oxide on Cu-8Cr-4Nb is poorly protective, but porosity diminished with progress of oxidation so that the terminal-stage oxidation product was dense, blocky, and protective.

The validity of this interpretation (assigning two kinetic stages in Fig. 7) was checked by statistical analysis for the region 800-900°C, at 25°C intervals. The result is summarized in Table 1. Column 2 gives the duration of Regime I, the fast initial stage of oxidation; the next column gives the duration of Regime II (terminal stage); and the next columns give Regimes I and II k_p values, and their ratios. The k_p values were determined by linear regression, one of the criteria of fit being an R^2 value of 0.995 or better. In cases where multiple measurements were made, the average values are shown in parenthesis. The combined durations of Regimes I and II do not add up to 50 hours because the earliest oxidation stage and the time of transition from I to II were omitted. There seems to be a trend towards a lengthening of Regime II duration with increasing temperature (at the expense of Regime I) up to a point. Except for the highest temperatures (875 and 900°C) where Zone I is practically absent, the ratio $k_{p(I)}/k_{p(II)}$ is fairly constant.

The Oxides

At all temperatures the oxide was comprised mainly of a thick scale of Cu_2O, topped by a film of CuO, the two layers being in the thickness ratio of 20:1 in most cases. Whiskers were observed on top of the CuO veneer, especially on oxides grown below ~750°C, the whisker profusion increasing at lower temperatures. For NARloy-Z and Cu both the CuO and Cu_2O layers appeared to be comparably dense; but for Cu-8Cr-4Nb the inner oxide

(Cu_2O) always exhibited a porous inner region and a dense outer region, presumably giving rise to the two different oxidation rates described earlier.

Fig. 8 compares oxide scales that grew on the three materials at 800°C. In each case the oxide-substrate boundary is to the right and marked with a block arrow; the gas interface is to the left. The total oxide thickness after 50 hours was 890 μm on Cu-8Cr-4Nb, 520 μm on NARloy-Z, and 490 μm on Cu. Cu-8Cr-4Nb produced the least homogeneous oxide, followed by Cu. In all 800°C oxides on Cu-8Cr-4Nb the inner (porous) region and outer (dense) region were found to be of about the same thickness. That lends further support to the correlation suggested earlier between the bifurcation of kinetics and oxide morphological changes. Oxide thickness, Δx, is related to oxidation time through the parabolic rate constants k_x as follows:

$$(\Delta x)^2 = A + k_x t. \qquad (1)$$

Omitting the constant term (which only corrects for a pre-existing oxide film) it becomes:

$$(\Delta x)^2 = k_x t. \qquad (2)$$

Since the oxide-thickening rate constant, k_x, is related to the weight-gain parabolic rate constant, k_p, by a mere scaling constant, α, eq. 2 reduces to:

$$(\Delta x)^2 = \alpha k_p t, \qquad (3)$$

Hence, if suffix 1 applies to Regime I and 2 to Regime II, eqn. 3 yields:

$$\frac{(\Delta x_1)^2}{(\Delta x_2)^2} = \left(\frac{k_1}{k_2}\right) \cdot \left(\frac{t_1}{t_2}\right). \qquad (4)$$

At 800°C the dense and porous oxide layers are of roughly equal thickness (Fig. 8), and one can write:

$$\left(\frac{k_1}{k_2}\right) = \left(\frac{t_2}{t_1}\right) \qquad (5)$$

In Table 1 $k_I/k_{II} \sim 2.8$ at 800°C, while $t_{II} = 30$ hours and $t_I = 3$ hours, giving $t_{II}/t_I \sim 3.0$ – in agreement with eq (5).

The XRD results shown in Table 2 revealed single and mixed (spinel) oxides of Cr and Nb beneath the scale. X-ray scans of the oxide scale from the top detected only CuO and Cu_2O; but when the oxide scale was removed from the substrate, the diffraction peaks from the non-Cu oxides became strong enough for identification. Fig. 9 is the profile of a sample oxidized at 800°C. The sample cross-section after removal of the main oxide overburden ($CuO+Cu_2O$) is shown in Fig. 9(a), and the EDS line scan along the dotted line is shown in Fig. 9(b). The Cu peaks were suppressed in 9(b) to fit them on the same vertical scale as the other elements. Both Figs. 9(a) and (b) reveal a film of secondary oxides (Cr-Nb oxides) hugging the contour of the substrate. The Cu profile in Fig. 9(b) exhibits minima at the surface (Cr-Nb-O) layer and at points that coincide with Cr and Nb peaks from the Cr_2Nb precipitates. Alongside the Cr-Nb-O layer is a denuded band – a narrow strip that is devoid of precipitates. The configuration of secondary oxide film, matrix, and precipitates is accentuated in Fig. 10, which shows a higher-magnification image of the area with corresponding maps of Cu, Cr, and Nb distribution. It confirms that the secondary oxide layer has Cr and Nb (and O) but no Cu, while the denuded band has only Cu.

The Cu matrix in this material would be expected to oxidize in the same way as pure Cu, by outward diffusion of Cu^+ through the oxide scale as the rate limiting event [4]; and the precipitates probably react with oxygen that has diffused through the oxide scale to the substrate interface, in the manner proposed for Cu-Cr and Cu-Nb alloys [7-9]. Oxidation of the Cr_2Nb precipitates best explains the enhanced oxidation resistance of Cu-8Cr-4Nb at intermediate temperatures, since these precipitates are the only point of difference from pure Cu. That explanation relates to the consumption of extra oxygen to convert Cr_2Nb to the mixed oxides. It is not possible to quantify this contribution to oxidation retardation without knowing all competing reactions so that oxygen consumption may be partitioned correctly. However, an analogy may be made to familiar systems. For instance, SiC and Si both have SiO_2 as their only condensed oxidation product and both reactions have the

same activation energy, 118 kJ/mol [16]; yet the oxidation of SiC is 2 -5 times slower than that of Si and the difference is attributed to consumption of the extra oxygen needed to convert the carbon in SiC into CO [17]. While oxide scale thickening is controlled by inward diffusion of oxygen in Si oxidation and outward diffusion of copper in the present case, the principle is the same: secondary reactions retard the overall oxidation process by consuming extra oxygen.

Oxidation of Cu-8Cr-4Nb seems to differ somewhat from that of the Cu-Cr and Cu-Nb alloys studied by Chiang et al [7-9]. They suggested that the second phase (which was Cr or Nb) oxidizes *in-situ* in the Cu matrix. In the present case, however, it is clear that Cr and Nb must cross the denuded band in Figs. 9 and 10 to get oxidized at the substrate-Cu_2O boundary. This suggests that the Cr_2Nb precipitates dissociate into Cr and Nb ions, which diffuse through the Cu matrix in the denuded zone to react with oxygen beneath the primary scale. This raises a few possibilities regarding oxidation rate control in this alloy. Any of the steps involved in the secondary oxidation (viz: decomposition of Cr_2Nb, ionization of the atomic species, their diffusion through Cu, or their reaction with oxygen at the Cu_2O-substrate boundary) could be the rate-limiting step in Cu-8Cr-4Nb oxidation – rather than the outward diffusion of Cu^+ through the Cu_2O/CuO scale.

The rate-determining process is, of course, the one with the highest activation energy. While the activation energy for Cu-8Cr-4Nb oxidation appears higher than that for Cu oxidation (Fig. 6), the evidence is not strong: due to the ambiguities noted earlier, one cannot be certain that the two activation energies in this figure (98 and 85 kJ/mol) are significantly different. For comparison, results obtained by Chiang and Grimmett for the same systems are re-plotted in Fig. 11 (by permission of the Electrochemical Society), with the axes converted to MKS units as in this paper). There is an excellent agreement between the present results and their k_p values for Cu-8Cr-4Nb oxidation. (The data in Fig 6 for final-stage Cu-8Cr-4Nb oxidation should be left out of this comparison, since it applies to long oxidation times which were not explored by Chiang and Grimmett.)

However, the results of Chiang and Grimmett fail to shed light on the key question of whether activation energies for Cu-8Cr-4Nb and Cu oxidation are significantly different in the intermediate-temperature regime of interest here (≤700°C). The problem is that their plot for Cu (Fig. 11) is rendered as one straight line, while the temperature range of their study (482–816°C) actually spans two different activation energy regimes for Cu. Of their four data points for Cu, the lowest belongs to the intermediate-temperature regime, while the other three belong to the high-temperature regime. The correct interpretation of Cu data is shown in Fig. 1 (which agrees with ref. 4). With only one Cu datum point in the intermediate temperature regime, the data of Chiang and Grimmett is too sparse for a proper regression to compare with the Cu plot in Fig. 6. Hence, Fig. 6 has to be taken at face value, and it indicates similar activation energies for Cu-8Cr-4Nb and Cu oxidation at intermediate temperatures but not at high temperatures. Above ~700°C Cu-8Cr-4Nb oxidation energy is somewhat lower for the initial oxidation stage but becomes higher in the terminal stage. The implication is that rate-controlling steps may be different for the two materials. Still, it is more likely that the accuracy achieved in this study is inadequate for a categorical conclusion on this point.

If oxidation of the second-phase precipitates is responsible for suppressing the aggregate oxidation kinetics in this alloy, it remains to be explained why this suppression seems to be ineffective at high temperatures. A likely explanation is that the same effect exists at higher temperatures but is overridden by other factors, such as diffusion rates that are now greatly increased for various reasons – including the prominence of a porous inner oxide zone.

Conclusions

The oxidation behavior of Cu-8Cr-4Nb in oxygen (and in air) differs significantly from that of Cu and NARloy-Z in many respects: (1) its rates are an order of magnitude slower in the interval 500 to ~700°C, but increase at higher temperatures to values comparable to that of Cu; (2) the increase of Cu-8Cr-4Nb oxidation rates at higher temperatures is accompanied by bifurcation into two kinetic regimes: a fast rate (several times faster that that of Cu) for the first ~10 hours of oxidation, and a slower rate (equal to that of Cu) in

the final stage of oxidation; (3) correspondingly, the inner (early) oxide growth is highly porous and hence poorly protective, while the outer (final) oxide is dense and blocky; (4) a layer of mixed Cr and Nb oxides separates the main scale, which corresponds to the oxides of copper, from the Cu-8Cr-4Nb substrate – and formation of this "secondary" oxide film is thought to be responsible for the reduced oxidation rates of Cu-8Cr-4Nb below ~700°C.

Acknowledgment

GRCop-84 (Cu-8Cr-4Nb) and NARloy-Z samples were provided by D.L. Ellis of Case Western Reserve University, and the TGA exposures were performed by D.L. Humphrey of QSS, Inc. Their assistance is highly appreciated. The author also wishes to thank J.L. Smialek for useful discussions of this manuscript.

References

1. D.L. Ellis, G.M. Michal, and N.W. Orth, Scripta Met vol 24 (1990) 885
2. D.B. Morgan, T. Nguyentat, J.E. Franklin, and A.C. Kobayashi, "Investigation of Copper Alloy Combustion Chamber Degradation by Blanching", Proceedings of the Advanced Earth-to-Orbit Propulsion Technology Conference, NASA Marshall Space Flight Center, Huntsville, AL, May 13-15 1986.
3. A. Ronnquist and H. Fischmeister, J. Inst. of Metals, vol 89 (1960-61) 65-76
4. J. –H. Park and K. Natesan, Oxidation of Metals, vol 39 #s5/6 (1993) 411-35
5. S.K. Bose, S.K. Mitra, and S.K. Roy, "Oxidation of Copper Under StaticCharge Supply", Trans. Indian Inst. Metals, vol. 50 #1 (1997) 85-96
6. S.K. Roy, S.K. Mitra, and S.K. Bose, "Influence of an Externally Applied Static Charge on the Oxidation Kinetics of Copper", Oxidation of Metals, vol 49, #s 3/4 (1998)
7. K.T. Chiang, P.D. Krotz, and J.L. Yuen, Surface and Coatings Tech., 76-77 (1995) 14-19
8. K.T. Chiang and J.P. Ampaya, Surface and Coatings Tech., 78 (1996) 243-7
9. K.T. Chiang, K.J. Kallenborn, J.L. Yuen, and N.E. Paton, Mater. Sci. & Eng., A156 (1992) 85-90

10. K.T. Chiang and D.L. Grimmett, Electrochemical Society Proc., vol. 98-9 (1998) 489-99
11. R.J. Hanrahan, et al., "High Temperature Oxidation of Be-Modified Intermetallic Compounds of the Nb-Cr System", High Temperature Corrosion & Materials Chemistry III, ECS Proceedings vol. 2001-12, ed. E. Opila and M. McNallan, The Electrochem. Soc., Inc. (2001), 77-83
12. L.U.J.T. Ogbuji, "Sub-parabolic Oxidation Behavior of Silicon Carbide", J. Electrochem. Soc., vol. 145, No. 8 (1998) 2877-82
13. C.E. Lowell, et al., "COSP: A Computer Model of Cuclic Oxidation", Oxidation of Metals, vol. 36, Nos. 1-2 (1991), 81-112
14. C.S. Tedman, "The Effect of Oxide Volatilization on the Oxidation of Cr and Fe-Cr Alloys", J. Electrochem. Soc., vol. 113 No. 8 (1966) 766-8
15. E.J. Opila and R.E. Hann, "Paralinear Oxidation of CVD SiC in Water Vapor", J. Am. Ceram. Soc., **80** [1] (1997) 197-205
16. L.U.J.T. Ogbuji and E. Opila, "A Comparison of the Oxidation Kinetics of SiC and Si_3N_4", J. Electrochem. Soc., vol. 142 No. 3 (1995) 925
17. L. Filipuzzi and R. Naslain, "Oxidation Kinetics of SiC Deposited From CH_3SiCl_3 Under CVI Conditions", J. Mater. Sci., 27 (1992) 3330

Table Captions

Table 1, Durations and parabolic rate constants for the two kinetic regimes observed in the oxidation of Cu-8Cr-4Nb at high temperatures

Table 2, Oxides detected by XRD on Cu-8Cr-4Nb after oxidation at intermediate and high temperatures; the secondary (Cr and Nb) oxides were detected only after removal of the Cu_2O/CuO overburden

Figure Captions

Fig. 1 Arrhenius plot of the oxidation data for pure Cu at intermediate and high temperatures, showing activation energies in the two regimes

Fig. 2 Kinetic plots for NARloy-Z and Cu (the two benchmark materials for this study); their kinetics are effectively the same at intermediate and high temperatures

Fig. 3 Oxidation kinetic of Cu-8Cr-4Nb at representative temperatures: The kinetics are essentially parabolic, but split into two different parabolic regimes (I and II) at high temperatures.

Fig. 4 Arrhenius plot for Cu-8Cr-4Nb oxidation in air and oxygen, at all temperatures investigated, showing that the behavior is the same in both ambients

Fig. 5 Arrhenius plot of Cu-8Cr-4Nb, NARloy-Z, and Cu oxidation data: all three have comparable oxidation rates at high temperatures, but Cu-8Cr-4Cr oxidizes at considerably slower rates than the two materials below (~700°C)

Fig. 6 Arrhenius plot showing the complex kinetics of Cu-8Cr-4Nb oxidation (compared to Cu): slower rates at intermediate temperatures and a split at high temperatures into a fast branch (initial oxidation) branch and a slow branch (terminal kinetics)

Fig. 7 Plot showing the split of Cu-8Cr-4Nb oxidation kinetics into parabolic regimes I and II at 800°C, and SEM images from corresponding depths in the oxide. Images I and II have identical magnification; the inset (below I) is 10X higher.

Fig. 8 Comparison of oxides scales grown at 800°C on (a) Cu-8Cr-4Nb, (b) NARloy-Z, and (c) Cu; block arrows indicate the oxide/metal boundaries; the NARloy-Z oxide is dense and uniform, the Cu oxide is uniform, except for large pores, while the Cu-8Cr-4Nb oxide has two zones exhibiting different degrees of consolidation

Fig. 9 (a) SEM micrograph of Cu-8Cr-4Nb after removal of the Cu_2O/CuO scale grown at 800°C; (b) EDS scan across the secondary (Cr+Nb) oxides to the substrate

Fig. 10 Enlarged view of a portion of the SEM image in Fig. 9, accompanied by EDS maps showing the distribution of Cu, Cr, and Nb

Fig. 11 Reproduction of Fig. 4, ref. 10 (with permission of the Electrochemical Society), for oxidation of Cu-8Cr-4Nb and Cu; since only one activation energy is indicated in this plot for Cu oxidation in the whole interval, it cannot be directly compared to the oxidation mechanisms suggested in the present work

Fig. 1

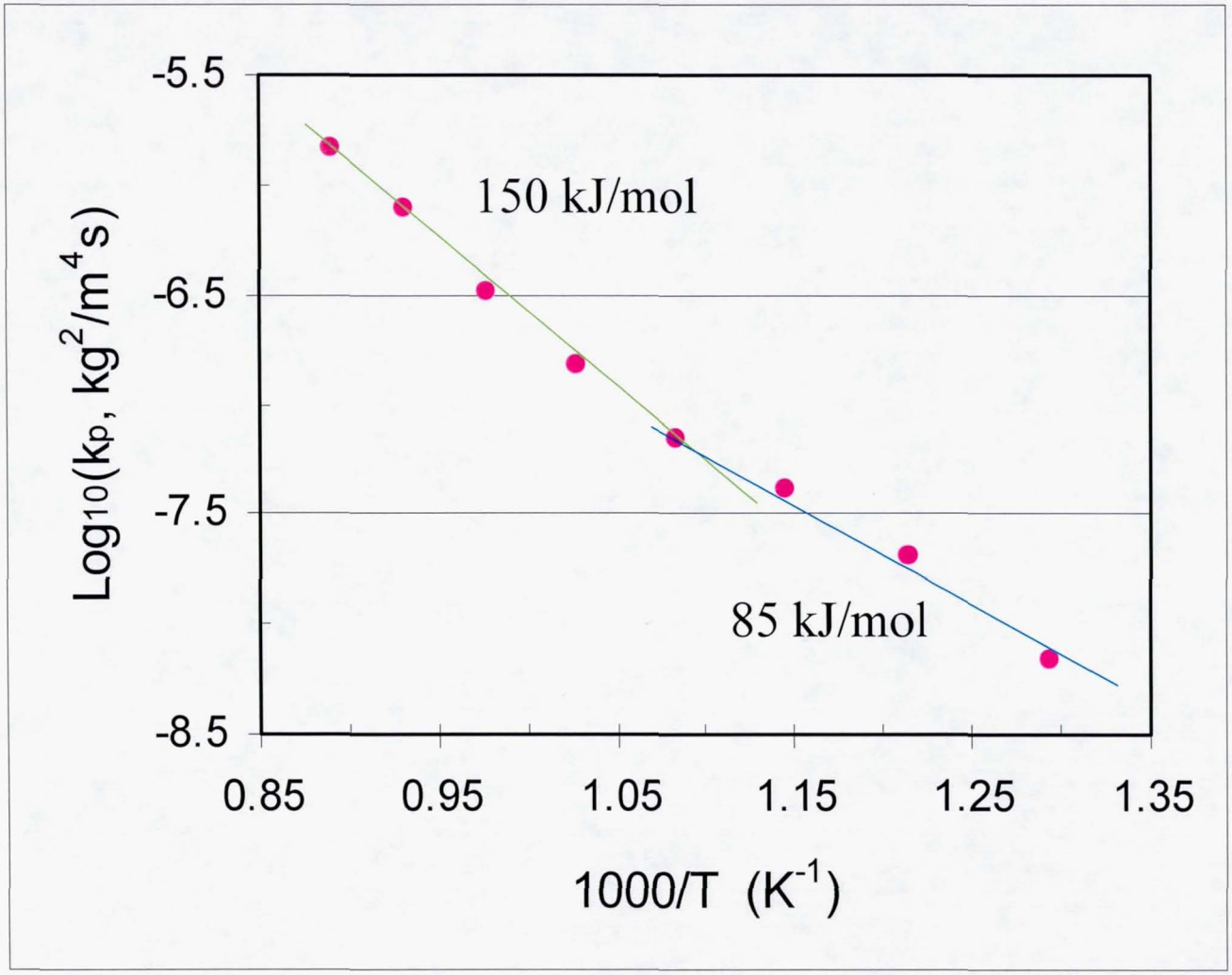
-5.5
-6.5
-7.5
-8.5
Log10(kp, kg2/m4s)
150 kJ/mol
85 kJ/mol
0.85
0.95
1.05
1.15
1.25
1.35
1000/T (K-1)

Fig. 1

Fig. 2

Oxidation behavior of NARloy & Cu are Same at Hi & Lo Temps

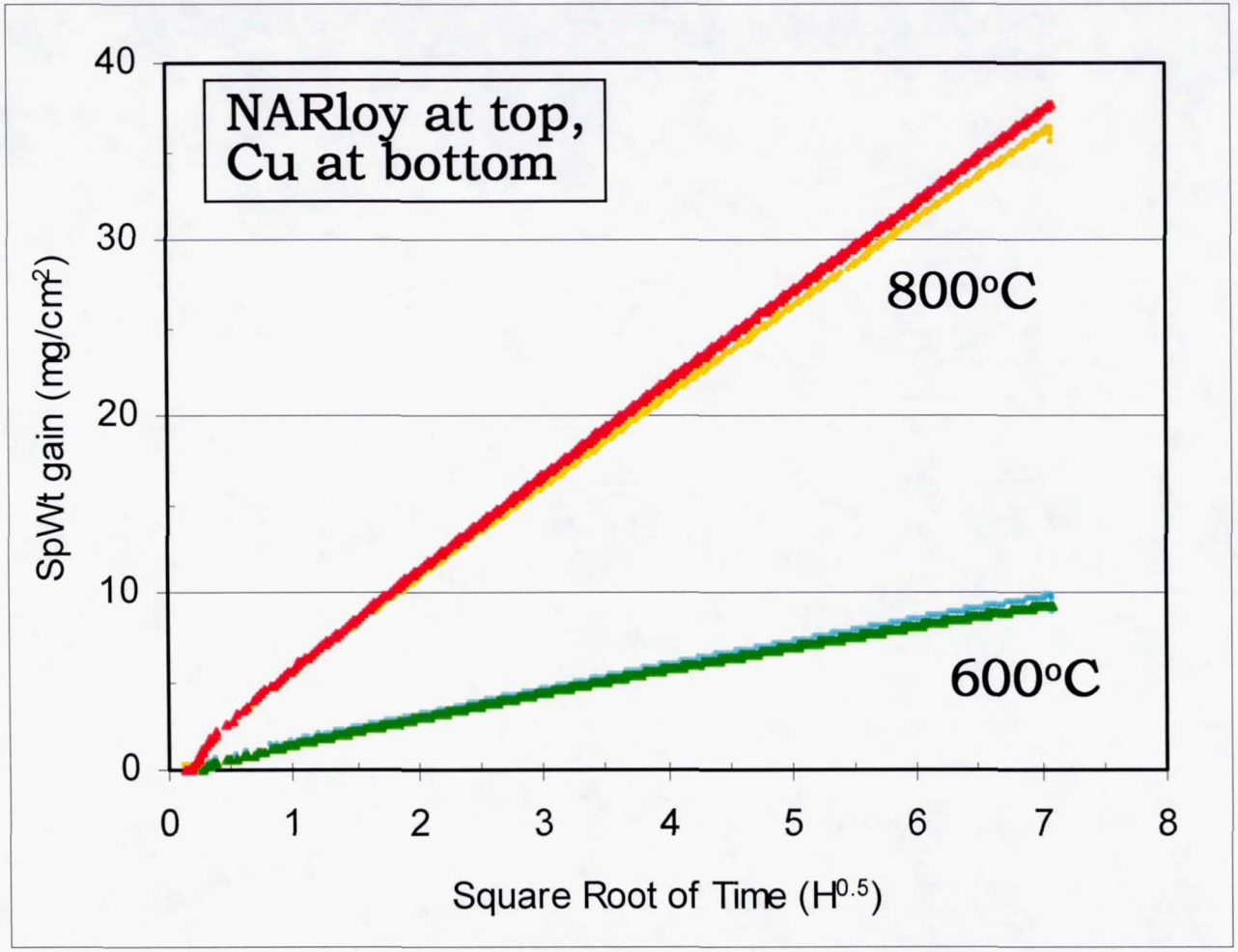

Fig. 2

~~Fig. 4~~

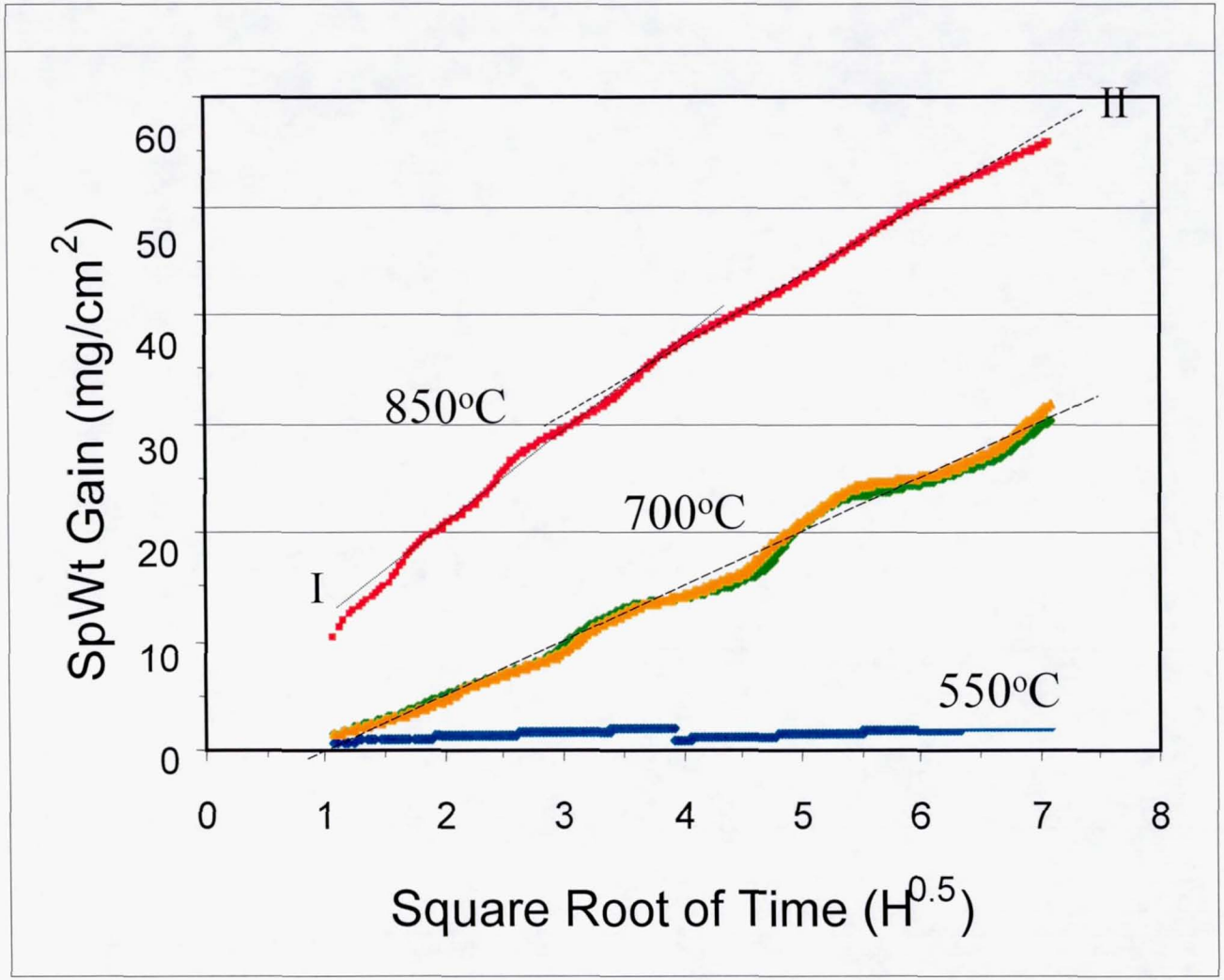
SpWt Gain (mg/cm^2)
60
50
40
30
20
10
0
0
1
2
3
4
5
6
7
8
Square Root of Time ($H^{0.5}$)
850°C
700°C
550°C
I
II

Fig. 3

Fig. 5

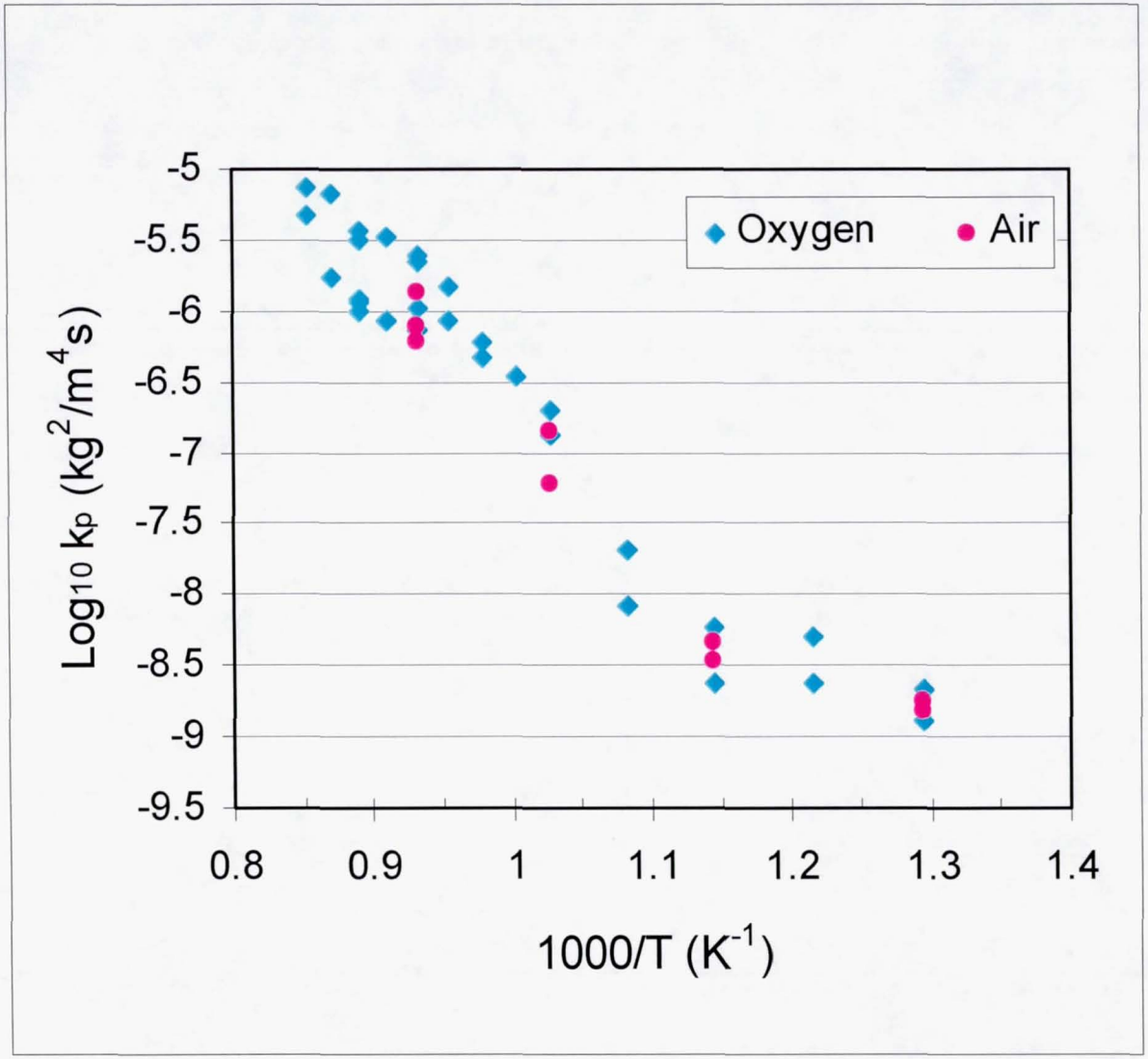
Oxygen
Air
-5
-5.5
-6
-6.5
-7
-7.5
-8
-8.5
-9
-9.5
0.8
0.9
1
1.1
1.2
1.3
1.4
Log10 kp (kg2/m4s)
1000/T (K-1)

Fig. 4

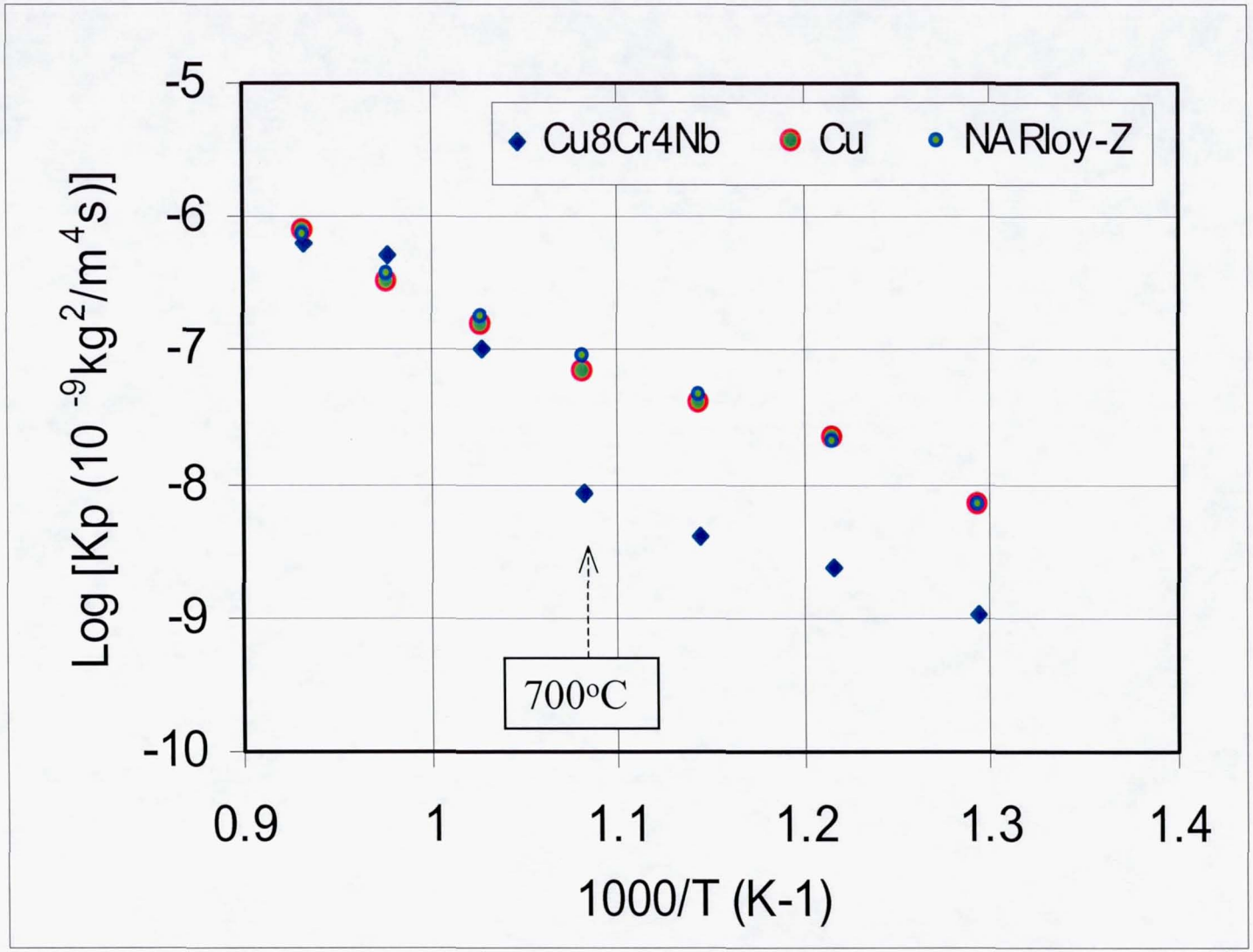
Cu8Cr4Nb
Cu
NARloy-Z
Log [Kp (10 -9kg2/m4s)]
-5
-6
-7
-8
-9
-10
0.9
1
1.1
1.2
1.3
1.4
1000/T (K-1)
700°C

Fig. 5

Fig. 6

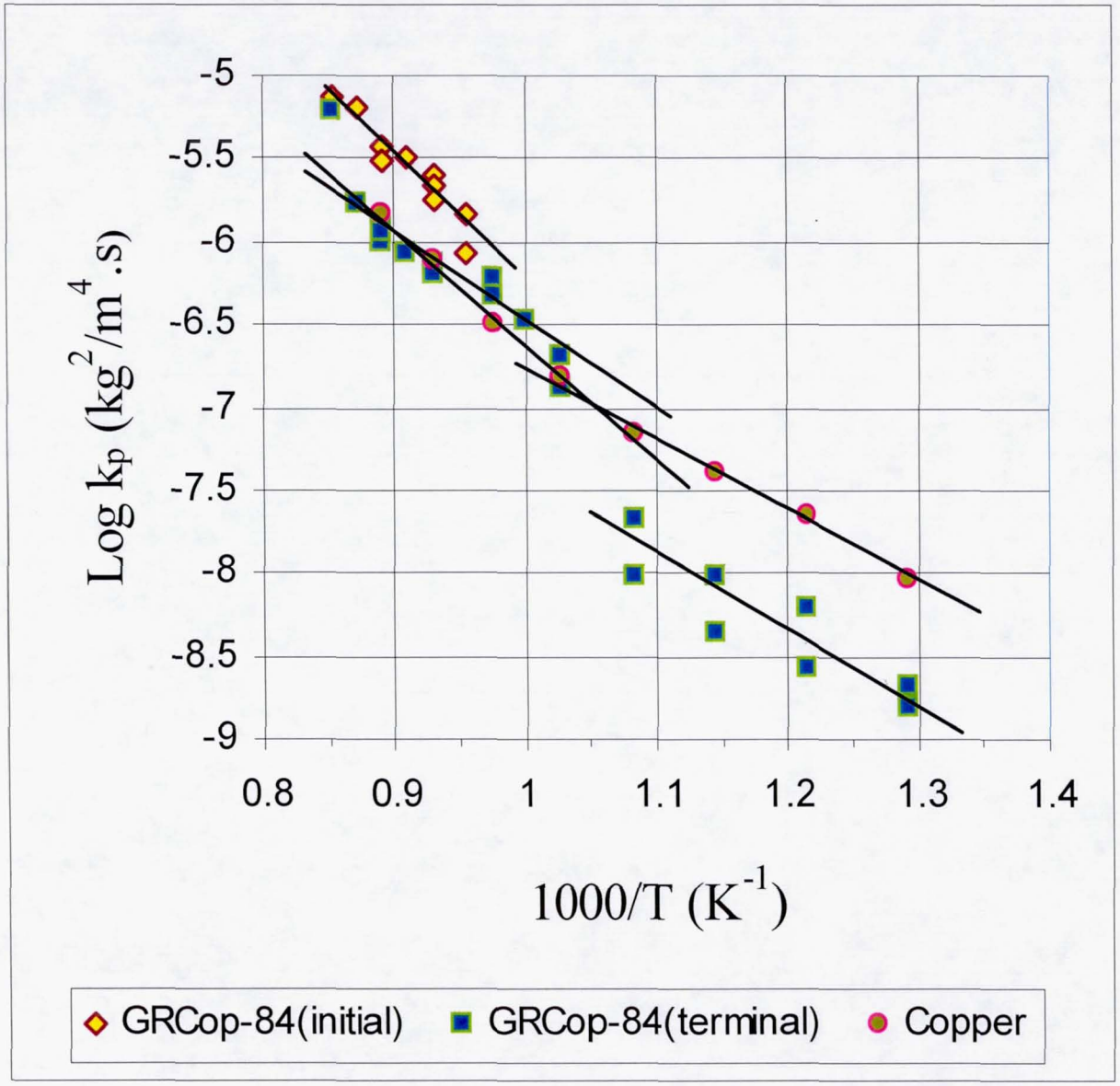
-5
-5.5
-6
-6.5
-7
-7.5
-8
-8.5
-9
Log k_p ($kg^2/m^4.s$)
0.8
0.9
1
1.1
1.2
1.3
1.4
1000/T (K^{-1})
GRCop-84(initial)
GRCop-84(terminal)
Copper

Fig. 6

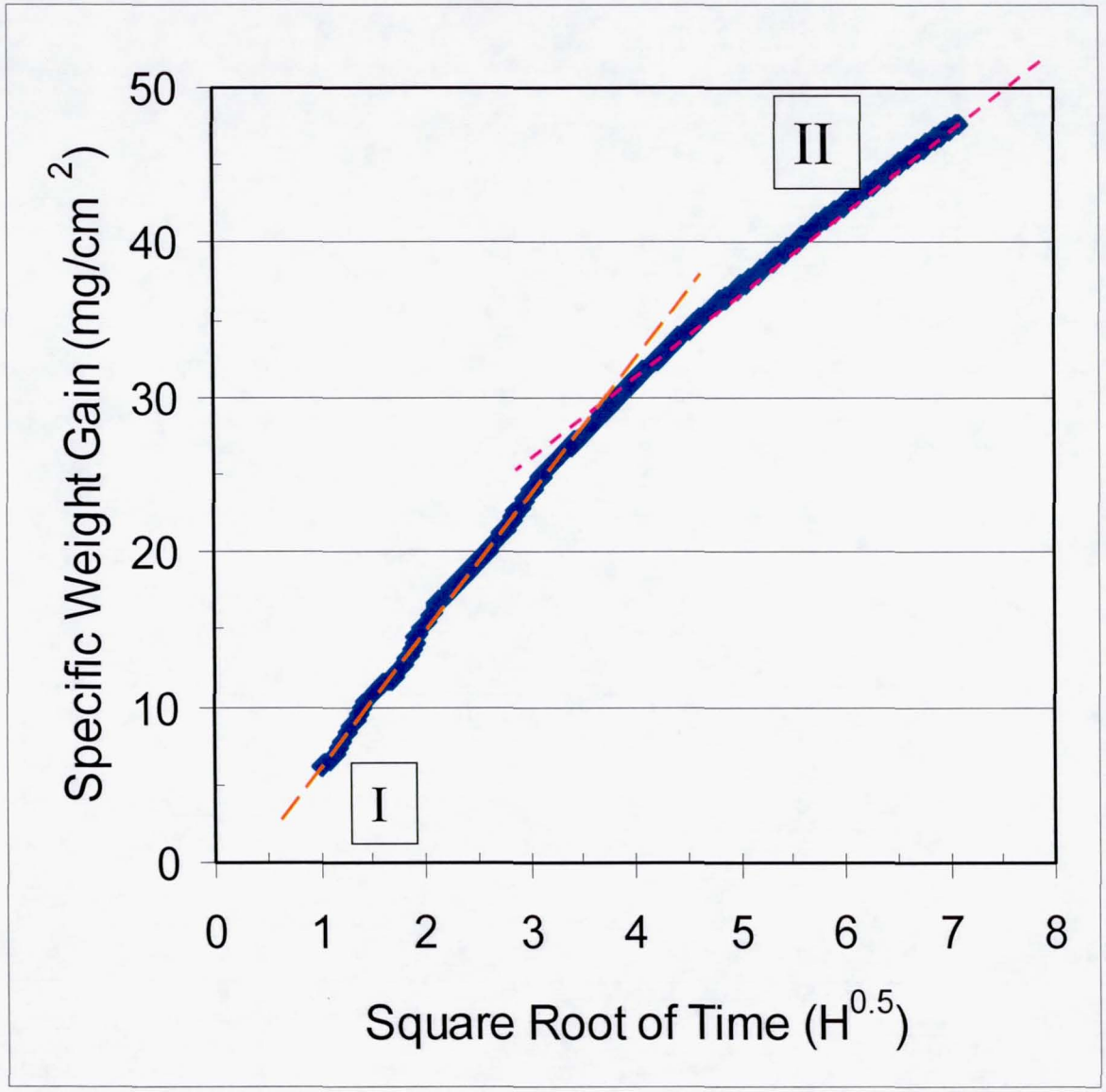
Specific Weight Gain (mg/cm 2)
50
40
30
20
10
0
0
1
2
3
4
5
6
7
8
Square Root of Time (H0.5)
II
I

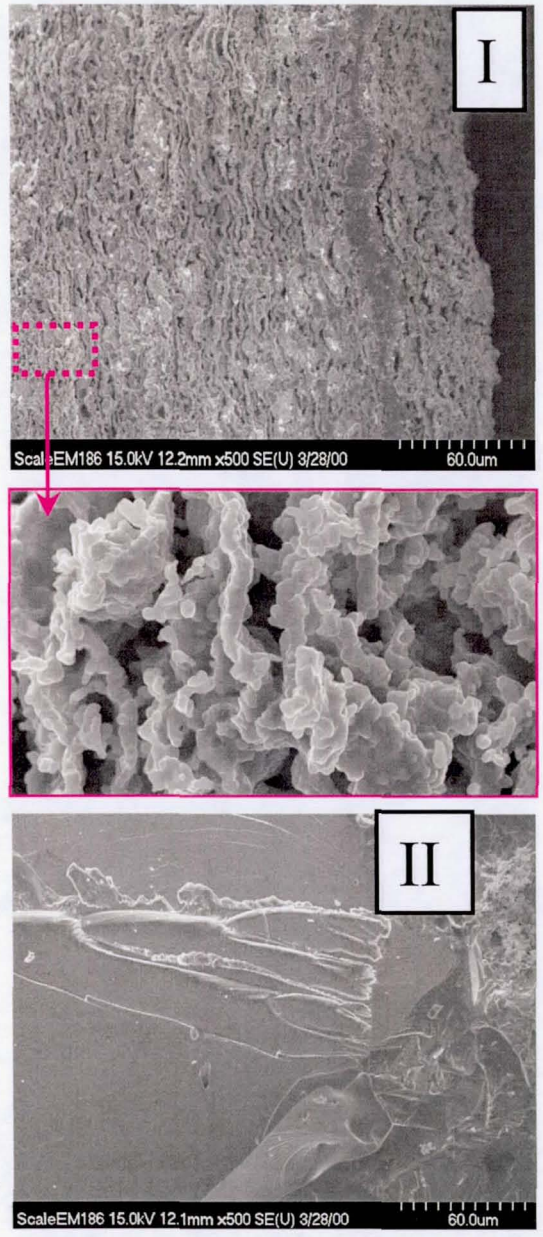
I
ScaleEM186 15.0kV 12.2mm x500 SE(U) 3/28/00
60.0um
II
ScaleEM186 15.0kV 12.1mm x500 SE(U) 3/28/00
60.0um

Fig. 7

Temp. (°C)	Regime I (H) **(av)**	Regime II (H) **(av)**	K_I (10^{-6} kg^2/m^4s) **(av)**	K_{II} (10^{-6} kg^2/m^4s) **(av)**	K_I / K_{II} **(av)**
800	10 10 12 12 12 **(10)**	25 30 28 35 0 (15-H run) **(30)**	1.97 2.16 1.78 1.96 1.89 **(1.95)**	0.630 0.748 0.625 0.868 **(0.72)**	3.1 2.9 2.8 2.52 **(2.83)**
825	10	30	2.564	0.865	**2.96**
850	9 10 7 **(9)**	30 25 30 **(28)**	2.82 3.08 3.12 **(3.13)**	0.978 1.14 1.21 **(1.10)**	2.88 2.70 2.61 **(2.73)**
875	4	43	6.55	4.86	**1.35**
900	2	45	7.24	5.91	**1.23**

Table 1

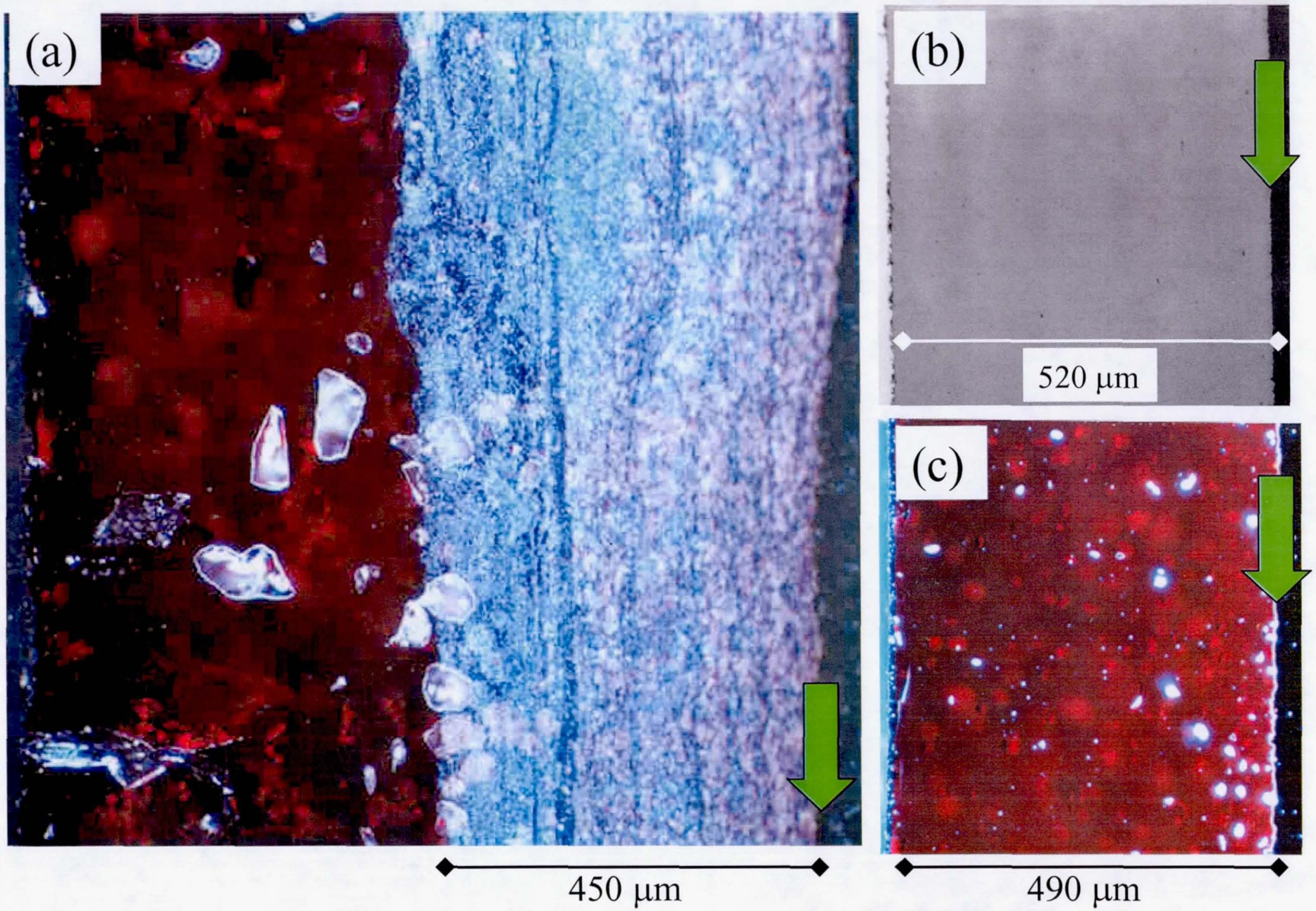
(a)
450 μm
(b)
520 μm
(c)
490 μm

Table 2

Temp (°C)	Whole Sample	Oxide Scale Removed From Substrate		
		Scale, from Top	Scale, from Bottom	Substrate, from Top
650		CuO Cu_2O	Cu_2O $CuNb_2O_6$ (probable) $CuCrO_2$ (possible) CrO_2 (possible)	
750		CuO Cu_2O	Wafer sample, completely converted to oxide	
800	CuO Cu_2O		$CrNbO_4$ $CuCrO_4$ $CuNb_2O_6$	$CrNbO_4$ $CuCrO_2$ $CuNb_2O_6$ Cr_2O_3 (possible) Cu
850		CuO Cu_2O (minor)	$CrNbO_4$ $CuCrO_4$ $CuNb_2O_6$	$CrNbO_4$ $CuCrO_2$ Cr_2O_3 (probable) Cu
875	CuO Cu_2O		$CrNbO_4$ Unidentified Spinel oxide (a_0=8.05)	$CrNbO_4$ Unidentified spinel Cr_2O_3 (probable) Cu
900	CuO Cu_2O		Cu_2O (probable) $CuCrO_2$ (probable)	$CrNbO_4$ Cr_2O_3 (probable) Cu

600-C oxide could not be removed from substrate for XRD

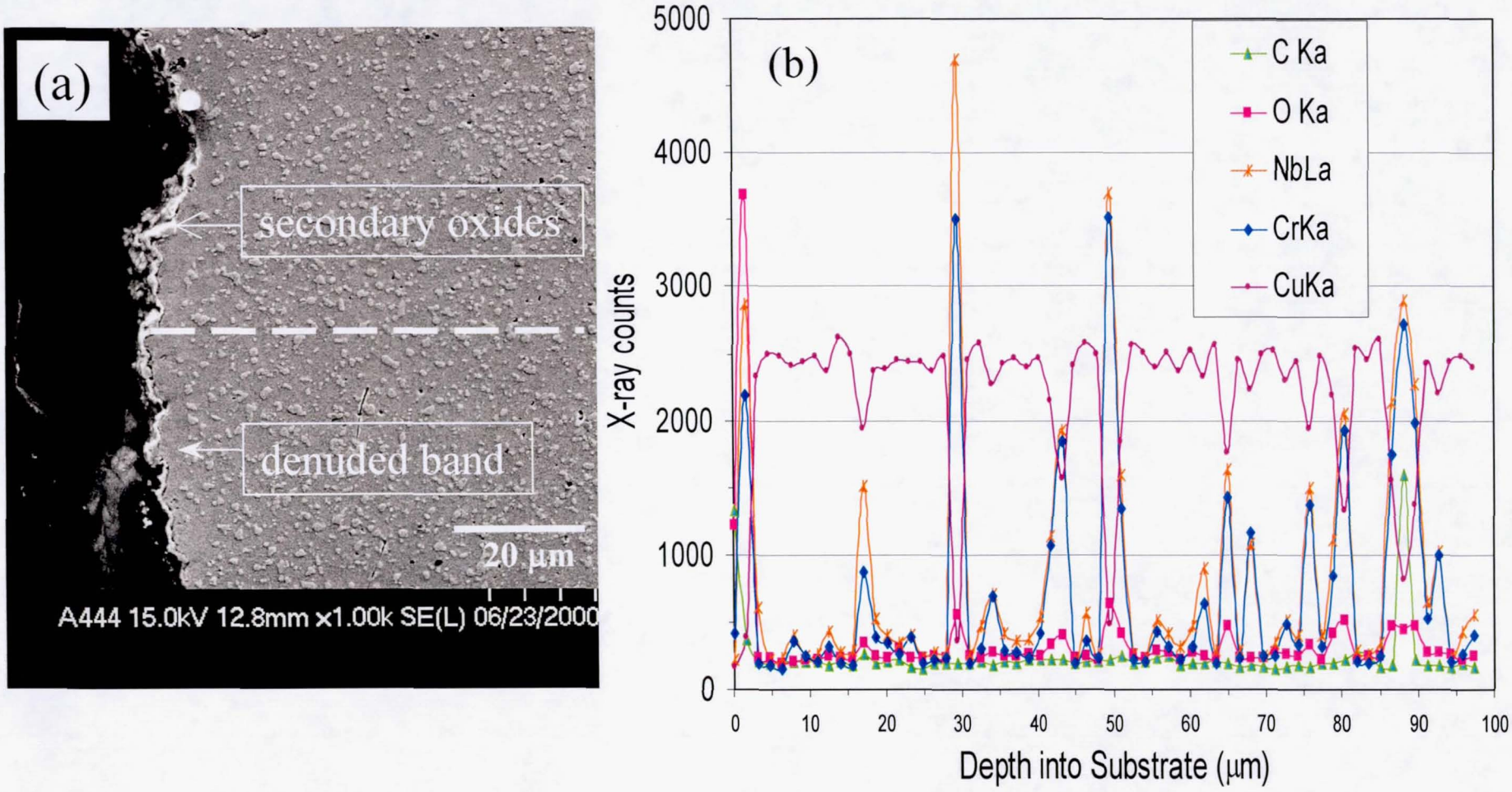
(a)
secondary oxides
denuded band
20 µm
A444 15.0kV 12.8mm x1.00k SE(L) 06/23/2000
(b)
C Ka
O Ka
NbLa
CrKa
CuKa
X-ray counts
5000
4000
3000
2000
1000
0
0
10
20
30
40
50
60
70
80
90
100
Depth into Substrate (µm)

Fig. 9

Fig. 10

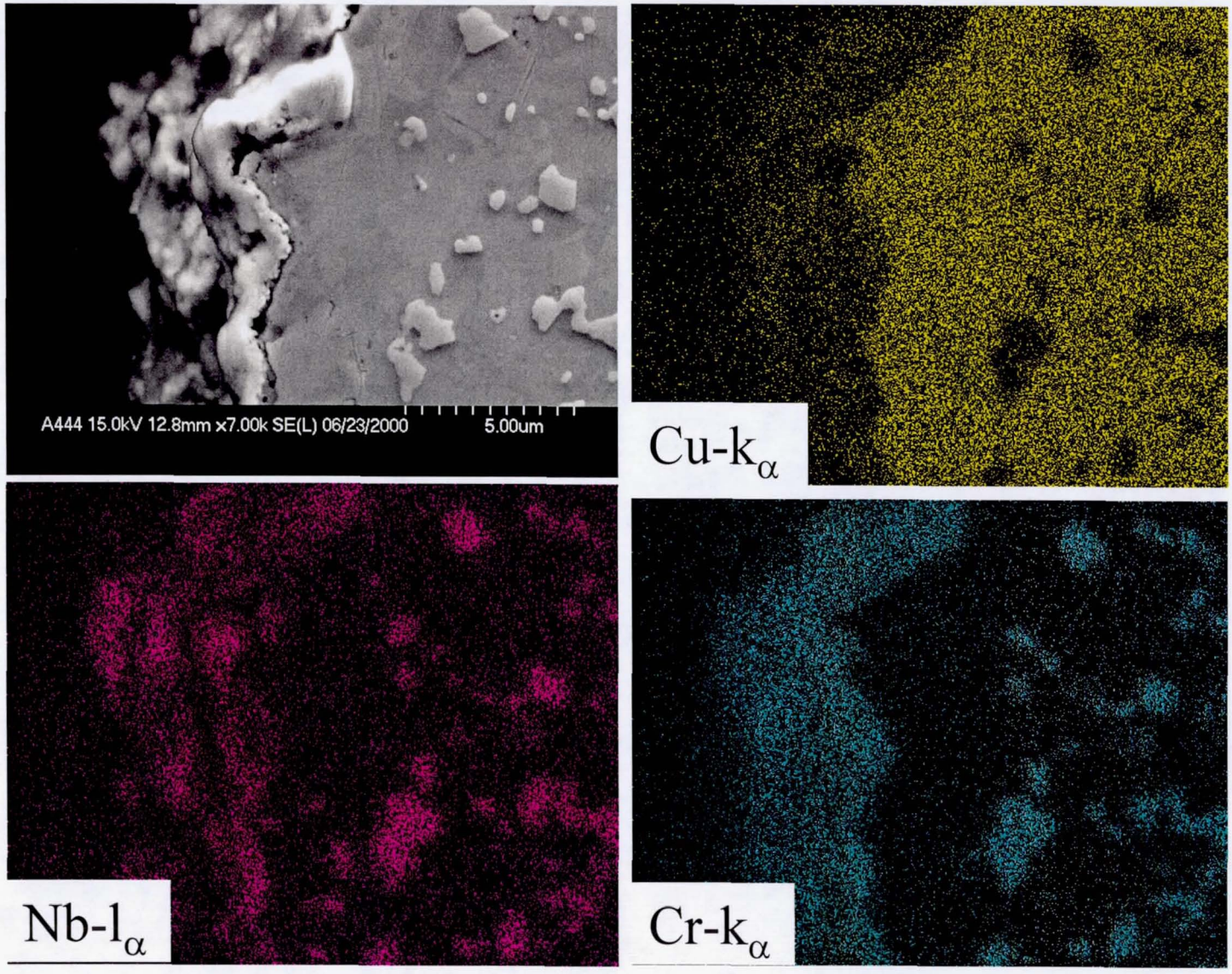
A444 15.0kV 12.8mm x7.00k SE(L) 06/23/2000
5.00um
Cu-k$_\alpha$
Nb-l$_\alpha$
Cr-k$_\alpha$

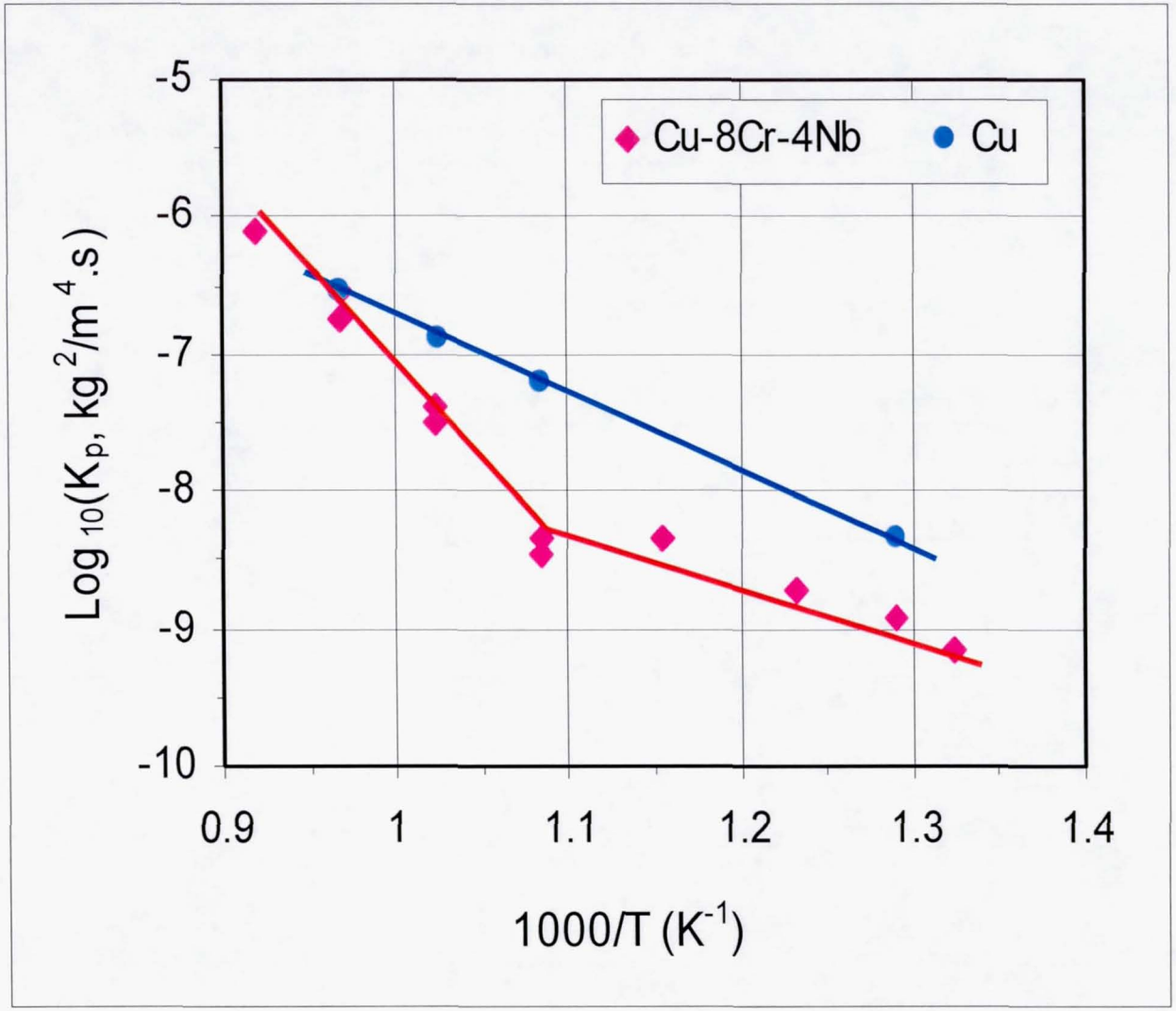

Fig. 11